ADVANCED FUNCTIONAL MATERIALS
www.afm-journal.de

Materials Views
www.MaterialsViews.com

The Multistep Tunneling Analogue of Conductivity Mismatch in Organic Spin Valves

*T. Lan Anh Tran, T. Quyen Le, Johnny G. M. Sanderink, Wilfred G. van der Wiel, and Michel P. de Jong**

Carbon-based, molecular semiconductors offer several attractive attributes for spintronics, such as exceptionally weak spin-orbit coupling and compatibility with bottom-up nanofabrication. In spite of the promising properties of organic spin valves, however, the physical mechanisms governing spin-polarized conduction remain poorly understood. An experimental study of C_{60}-based spin valves is presented and their behavior is modeled with spin-polarized tunneling via multiple intermediate states with a Gaussian energy distribution. It is shown that, analogous to conductivity mismatch in the diffusive regime, the magnetoresistance decreases with the number of intermediate tunnel steps, regardless of the value of the spin lifetime. This mechanism has been largely overlooked in previous studies of organic spin valves. In addition, using measurements of the temperature and bias dependence of the magnetoresistance, inhomogeneous magnetostatic fields resulting from interfacial roughness are identified as a source for spin relaxation and dephasing. These findings constitute a comprehensive understanding of the processes underlying spin-polarized transport in these structures and shed new light on previous studies of organic spin valves.

1. Introduction

Controlling and probing charge carrier spin polarization via electrical means is an attractive route towards the development of practical semiconductor spintronic devices,[1,2] which are expected to have a strong impact on future information processing and storage technologies. Considerable success has been obtained over the last number of years in the field of inorganic semiconductor spintronics, with the demonstration of, for example, the creation and detection of a robust spin polarization in silicon at room temperature.[3] Key to this success is the growing understanding of the physical mechanisms that govern the spin-dependent behavior of charge carriers in ferromagnetic-metal/semiconductor heterostructures,[2] and in particular of the practical limitations[4] for spin-polarized charge carrier injection and detection using ferromagnetic metal contacts, e.g., conductivity mismatch in the diffusive transport regime.[5]

The field of organic semiconductor spintronics[6–8] is lagging behind considerably in this respect, as the physics underlying spin-polarized transport in organic devices remains somewhat elusive. This is unfortunate, since carbon-based, organic semiconductors offer a number of unique advantages,[6,7] such as potentially very long spin lifetimes,[9,10] bottom-up fabrication relying on self-assembly, and non-stringent requirements for interface formation and film growth, which allow for, for example, vertical stacks comprising alternating layers of ferromagnetic metals and molecular semiconductors. Large magnetoresistance effects have been reported in such organic-based vertical spin valves,[11] comprising e.g., thin films of organic molecules[7] and fullerenes,[12–14] in several cases also at room temperature.[12,15] As is fairly well established, the electronic structure of the hybrid interfaces plays an important role.[16,17] It remains unclear, however, if the limitations for spin-polarized charge injection and detection in inorganic semiconductors are applicable to organic spin valves as well, since these often show electrical characteristics that are indicative of multistep tunneling.[7,18,19] In this regime, charge carriers tunnel via a limited amount of steps involving localized intermediate states in the organic semiconductor,[19] and a description in terms of diffusive transport fails. Nevertheless, the junction magnetoresistance (JMR) is found to be very sensitive to the thickness of the organic semiconductor layer, and the suppressed JMR in the transition from tunneling transport to a regime limited by bulk hopping conduction has been attributed to "conductivity mismatch" by several authors.[13,18,20] Another issue that remains subject to debate is how spin relaxation and dephasing take place in the organic semiconductor and how this affects the JMR. Spin precession in the random hyperfine fields of hydrogen nuclei has been shown to play an important role in the phenomenon of organic magnetoresistance[21] and has been proposed to affect the JMR of organic spin valves.[19]

Here, we address these important issues using a joint experimental and modeling study of vertical spin valves comprising ultrathin (up to 20 nm) C_{60} layers (see Experimental Section for details). We show that multistep tunneling leads to a behavior

T. L. A. Tran, T. Q. Le, J. G. M. Sanderink, Prof. W. G. van der Wiel, Dr. M. P. de Jong
NanoElectronics Group
MESA+ Institute for Nanotechnology
University of Twente
7500 AE Enschede, the Netherlands
E-mail: M.P.deJong@utwente.nl

DOI: 10.1002/adfm.201102584

analogous to conductivity mismatch,[5] in the sense that the inclusion of an increasing number of intermediate tunneling steps results in a more and more spin-independent junction resistance, regardless of the spin lifetime and spin diffusion length. This previously overlooked fact places numerous published studies on organic spin valves in an entirely new light, including those on similar junctions based on C_{60}.[12,13] Moreover, it explains the salient features of such devices, namely a strong dependence of the JMR on the organic layer thickness and on temperature, and reconciles the expectation of very long spin lifetimes in organic semiconductors with the relatively short length scales over which a finite JMR is observed.[7] Regarding these potentially long spin lifetimes, C_{60} is an attractive choice. Since C_{60} molecules are composed purely of carbon and the 99% predominant ^{12}C isotopes have zero nuclear spin, the effects of the above mentioned hyperfine fields are very small and may be neglected.[22,23] Here we show, however, that spin relaxation and dephasing nevertheless play a role and propose that inhomogeneous magnetic fields due to finite interfacial roughness are the cause of this.

2. Multistep Tunneling Calculations

We begin with a description of our model, and then turn to a comparison with experimental results. When the C_{60} thickness, d_C, is well below 10 nm, the charge transport can be described in a fairly straightforward manner, in terms of a superposition of direct- and two-step tunneling. We use the model as developed by Schoonus et al.[19] as a starting point, with several additions as outlined below.

2.1. Spin Polarized Tunneling via an Intermediate State

The model of Schoonus et al.[19] considers two-step tunneling processes, in our case involving intermediate states in the C_{60} layer, in addition to direct tunneling across a composite Al_2O_3/C_{60} barrier. In a two-step process (see **Figure 1**), electrons tunnel from the first ferromagnetic (FM) electrode (0), with tunnel spin polarization (TSP) p_0, into an intermediate state (1) within the C_{60} layer with time-averaged occupation numbers $n_\uparrow/n_\downarrow$ for spin up/down electrons, and subsequently into the second FM electrode (2), with TSP p_2. Back-tunneling processes are also considered, assuming a Fermi–Dirac distribution $f(E)$ and constant density of states (DOS) for the FM metals (this is a somewhat oversimplified but reasonable approximation for low bias voltages). The occupation number of a certain intermediate state in the C_{60} layer is determined by the equality of the inbound- and outbound tunneling rates under steady state conditions, $J_{01} = J_{12} = J_{\text{two-step}}$. The parameters that enter the model are p_0 and p_2, the thickness d_A and d_C of the Al_2O_3 and C_{60} layers, respectively, and the extinction coefficients of evanescent states κ (for Al_2O_3) and γ (for C_{60}). The extinction coefficients depend in turn on the barrier height U and the effective mass m_e in the evanescent state, via e.g., $\gamma = 2\sqrt{2m_e U}/\hbar$, where $\hbar$ is the reduced Planck constant. Further details can be found in ref. [19].

The effects of two-step tunneling via an intermediate state on the magnetotransport properties of the junctions can be described as follows. Considering a parallel magnetization

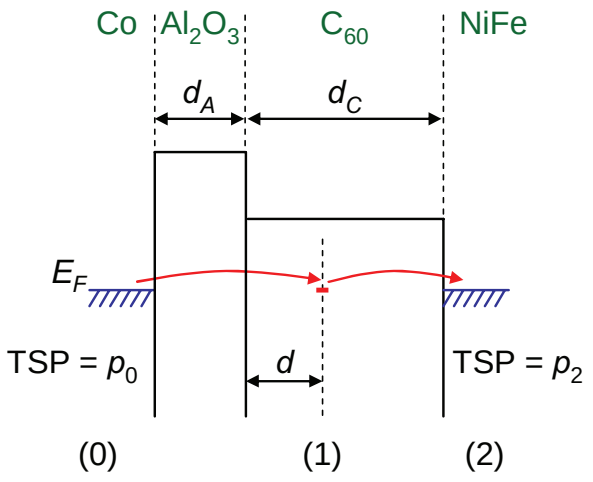

Figure 1. A two-step tunneling event involving an electron tunneling out of the Co electrode (0) into an intermediate state (1) in the C_{60} layer and subsequently into the NiFe counter electrode (2).

alignment for electrodes (0) and (2), the tunnel current density $J_{01\uparrow P}$ (with the label "P" for parallel magnetization) of majority spin (up) electrons flowing out of the FM contact (0) into the intermediate state (1) at a distance d from the Al_2O_3/C_{60} interface, is given by:

$$J_{01\uparrow P} \propto \tfrac{1}{2}(1+p_0)\left(1-n_{\uparrow P}\right)e^{-(\kappa d_A+\gamma d)} f(E_F) - \tfrac{1}{2}(1+p_0)\, n_{\uparrow P} e^{-(\kappa d_A+\gamma d)}\left(1-f(E_F)\right) \quad (1)$$

which is composed of a forward tunneling current proportional to $(1 - n_{\uparrow P})$ and a back tunneling current proportional to $n_{\uparrow P}$, while $\tfrac{1}{2}(1 + p_0)$ represents the fraction of the total current (due to both spin up and spin down electrons) consisting of spin up electrons tunneling out of the FM contact (0) at the Fermi energy, E_F. Here, the transmission of electrons through the Al_2O_3 and C_{60} layers, with thickness d_A and d_C, scales with the extinction coefficients for evanescent states κ and γ, respectively. The extinction coefficients, which depend on the barrier height and the effective mass in the evanescent state, can be estimated from measurements of the tunnel resistance (in the low bias, Ohmic regime) as a function of layer thickness.

For a certain bias voltage V applied over the junction (with a polarity such that electrons tunnel from electrode (0) via intermediate sites (1) into electrode (2)), the current density $J_{12\uparrow P}$ of carriers flowing out of the localized site in the C_{60} layer into FM contact (2), with TSP p_2, is

$$J_{12\uparrow P} \propto \tfrac{1}{2}(1+p_2)\, n_{\uparrow P} e^{-\gamma(d_C-d)}\left(1-f(E_F+eV)\right) - \tfrac{1}{2}(1+p_2)\left(1-n_{\uparrow P}\right)e^{-\gamma(d_C-d)} f(E_F+eV) \quad (2)$$

where e is the electron charge. Under steady state conditions, $J_{01\uparrow P} = J_{12\uparrow P} = J_{\uparrow P}$, which yields $n_{\uparrow P}$ such that the current density for tunnel processes involving intermediate sites at a distance d from the Al_2O_3 electrode can be evaluated:

$$n_{\uparrow P} = \frac{\tfrac{1}{4}(1+p_0)\, e^{-(\kappa d_A+\gamma d)} + \tfrac{1}{2}(1+p_2)\, e^{-\gamma(d_C-d)} f(E_F+eV)}{\tfrac{1}{2}(1+p_2)\, e^{-\gamma(d_C-d)} + \tfrac{1}{2}(1+p_0)\, e^{-(\kappa d_A+\gamma d)}} \quad (3)$$

Similar expressions can be obtained for the minority spin current $J_{01\downarrow P}$ related to $n_{\downarrow P}$, upon replacing p_0 with $-p_0$ and p_2 with $-p_2$, and for the antiparallel (AP) magnetization configuration, upon setting $p_0 = -p_0$ while keeping p_2 unchanged (or vice versa). The junction magnetoresistance (JMR) for tunneling via an intermediate site at a distance d within the C_{60} layer can then be evaluated as $JMR(d) = (J_P - J_{AP})/J_{AP}$, (note that this is equivalent to $(R_{AP} - R_P)/R_P$, where R is the resistance) with $J_P = J_{\uparrow P} + J_{\downarrow P}$, and $J_{AP} = J_{\uparrow AP} + J_{\downarrow AP}$.

After determining the equations for the spin polarized two-step tunneling currents as a function of the distance d of the intermediate site from the Al_2O_3/C_{60} interface, the JMR resulting from tunneling via en ensemble of states with a spatially homogeneous distribution is found by integrating the expressions for the current densities with respect to d. The magnetoresistance that results is considerably lower than that due to direct tunneling of electrons between contacts (0) and (2), given by $2p_0p_2/(1 - p_0p_2)$. The reason for this is that, in addition to the TSPs of the electrodes, the spin dependent occupation numbers also determine the tunneling rates.

Let us discuss a specific hypothetical case that illustrates this effect, and for which the analysis is especially simple. Consider a symmetric system, consisting of two identical FM electrodes with $p_0 = p_2 = p$, and a single localized state in the barrier, located exactly halfway between the electrodes. The spin dependent occupation numbers of the intermediate state are determined by the balance between inbound- and outbound tunneling events. Due to the symmetry of the system when the magnetization configuration is parallel, the transmission probabilities for tunneling into and out-of the localized state are equal. If we disregard back tunneling, and set the bias voltage to zero, the equations for the tunneling rates in the parallel magnetization configuration are:

$$J_{01\uparrow P} \propto \tfrac{1}{2}(1+p)\left(1-n_{\uparrow P}\right)e^{-\gamma d} = J_{12\uparrow P} \propto \tfrac{1}{2}(1+p)\,n_{\uparrow P}e^{-\gamma(d_C-d)} = J_{\uparrow P} \quad (4)$$

$$J_{01\downarrow P} \propto \tfrac{1}{2}(1-p)\left(1-n_{\downarrow P}\right)e^{-\gamma d} = J_{12\downarrow P} \propto \tfrac{1}{2}(1-p)\,n_{\downarrow P}e^{-\gamma(d_C-d)} = J_{\downarrow P} \quad (5)$$

Since the intermediate state is located exactly halfway between the electrodes, i.e., $(d_C - d) = d$, the exponential terms are equal. Therefore, since $J_{01\uparrow P} = J_{12\uparrow P}$ and $J_{01\downarrow P} = J_{12\downarrow P}$, it follows that $n_{\uparrow P} = n_{\downarrow P} = \tfrac{1}{2}$, for any value of $p < 1$. In the case $p = 1$ the spin down tunneling rates are equal to zero, and hence $n_{\uparrow P} = \tfrac{1}{2}$, $n_{\downarrow P} = 0$. When the electrodes are magnetized in the antiparallel configuration, the equations are:

$$J_{01\uparrow AP} \propto \tfrac{1}{2}(1-p)\left(1-n_{\uparrow AP}\right)e^{-\gamma d} = J_{12\uparrow AP} \propto \tfrac{1}{2}(1+p)\,n_{\uparrow AP}e^{-\gamma(d_C-d)} = J_{\uparrow AP} \quad (6)$$

$$J_{01\downarrow AP} \propto \tfrac{1}{2}(1+p)\left(1-n_{\downarrow AP}\right)e^{-\gamma d} = J_{12\downarrow AP} \propto \tfrac{1}{2}(1-p)\,n_{\downarrow AP}e^{-\gamma(d_C-d)} = J_{\downarrow AP} \quad (7)$$

where the magnetization of electrode (0) has been flipped. It follows that $n_{\uparrow AP} = \tfrac{1}{2}(1-p)$ and $n_{\downarrow AP} = \tfrac{1}{2}(1+p)$, for $p < 1$. For $p = 1$, the current in the antiparallel configuration is always equal to zero, due to the terms $(1 - p)$ in Equations (6) and (7). In addition, $n\uparrow_{AP} = 0$, $n\downarrow_{AP} = 1$ for $p = 1$, since electrode (0), now magnetized in the opposite direction, contains no spin up electrons at the Fermi level. Hence the magnetoresistance for $p = 1$ is infinite, as is the case for direct tunneling between to 100% polarized electrodes. However, for $p < 1$, inserting the spin dependent occupation numbers into Equations (4–7) for the tunneling rates gives a magnetoresistance $(J_P - J_{AP})/J_{AP}$, with $J_P = J_{\uparrow P} + J_{\downarrow P}$ and $J_{AP} = J_{\uparrow AP} + J_{\downarrow AP}$, proportional to $p^2/(1 - p^2)$, i.e., half that of direct tunneling between the two electrodes (as was also pointed out by Schoonus et al.).[19]

2.2. Tunneling via a Gaussian DOS of Intermediate States

We consider two-step tunneling via a Gaussian DOS of intermediate C_{60}-derived states, centered at the lowest unoccupied molecular orbital (LUMO) of C_{60}, in contrast to the uniform energetic distribution of states in the model of Schoonus et al. A similar picture is used routinely to describe charge transport in the hopping regime in (disordered) organic solids.[24,25] From previous experiments, the position of the LUMO with respect to E_F is well known: The high electron affinity of solid C_{60}, equal to 4.0 eV,[26–28] leads to Fermi level pinning on metallic substrates with a work function of 4.5 eV or smaller,[29] as is the case for the present electrodes, Co/Al_2O_3 and NiFe.[30] We set the Gaussian width, determined by inhomogeneous broadening, to a realistic value of 0.3 eV (full width at half maximum) via the parameter σ (see **Equation 1**), while the energy difference $E_F - E_{LUMO}$ is set to 0.5 eV. **Figure 2** shows schematic representations of two-step tunneling processes via a Gaussian DOS of intermediate states. Applying a bias voltage tilts the potential within the C_{60} layer, such that the DOS of intermediate states aligned with E_F of the electrode from which electrons are expelled becomes a strong function of d. Correspondingly, the current flowing under different bias conditions will involve two-step (or multistep at sufficiently large C_{60} thickness) tunneling via states that are distributed differently within the C_{60} layer. The two-step tunnel current density $J_{two\text{-}step}$ as a function of d and bias voltage V is:

$$J_{two-step}(V) = J_{two-step}(0)\,e^{-\left((E_F-E_{LUMO})-|eV|\frac{d}{d_A+d_C}\right)^2/\sigma} \quad (8)$$

for electrons tunneling from the left (Co/Al_2O_3 electrode) to the right (NiFe electrode), meaning under application of a negative potential in our experiments. For the opposite bias polarity, we substitute $(d_C - d)$ for d. $J_{two\text{-}step}(0)$, i.e., the two-step tunnel current density at zero bias, is calculated using Equation 1, 2, and 3.

2.3. Tunneling via Multiple Intermediate States

For increasing C_{60} thickness, the contribution of tunneling events that involve more than one intermediate site in the C_{60} layer will increase as the transmission probability for individual tunneling processes drops exponentially with the tunneling distance. For the sake of illustrating the main effects of tunneling via multiple intermediate sites on the magnetoresistance, we

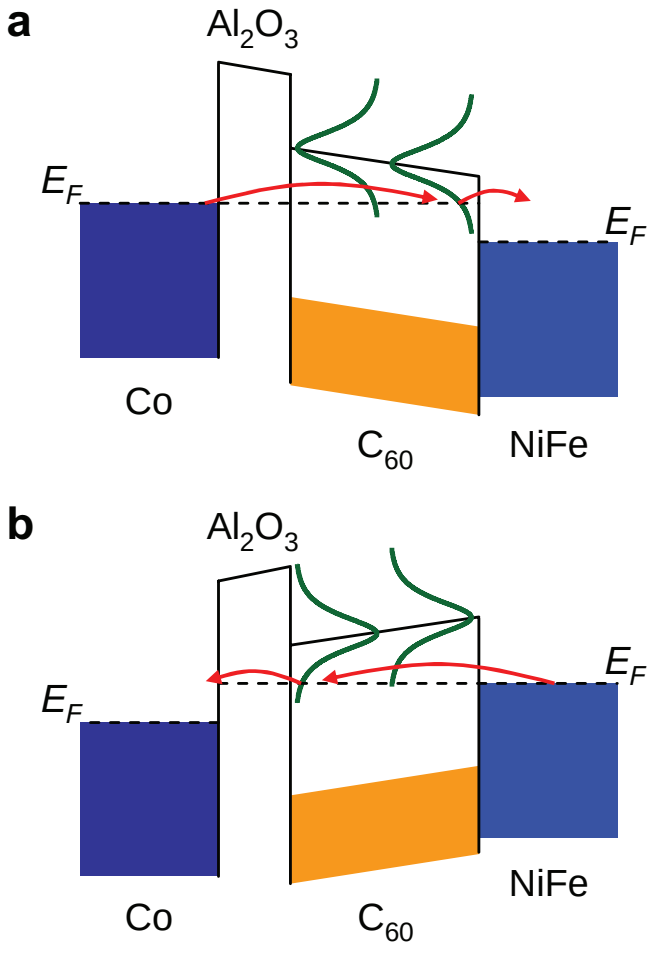

Figure 2. Two-step tunneling via intermediate states with a Gaussian energy distribution centered on the LUMO of C_{60}. Under application of a negative bias voltage (a), electrons tunneling out of the Co electrode at E_F encounter an increasing density of intermediate states at an increasing distance from the Al_2O_3 surface. A positive bias (b) results in an increased amount of states close to the Al_2O_3 surface for electrons tunneling out of the NiFe electrode.

limit ourselves in the discussion below to two simple cases that can be evaluated easily: 1) that of up to four intermediate tunneling sites within the barrier with equal probability for inbound versus outbound tunneling (i.e., equidistantly placed sites within the barrier) and 2) that of two sites near both electrodes (at the same distance from each electrode) connected via an arbitrary number of uncorrelated "hops" within the C_{60} layer.

2.3.1. Multiple Equidistant Tunneling Sites

When back tunneling is not taken into account, and only a single barrier (corresponding to the C_{60} layer) is considered, we can easily evaluate the case of equidistant tunneling events (with the same transmission probability) involving a limited number i of intermediate states. The problem to be solved, for arbitrary i, is that of the following set of equations:

$$\begin{aligned} &J_{01\uparrow P} \propto \alpha\left(1-n_{1\uparrow P}\right) = \\ &\ldots \\ &J_{i-2,i-1\uparrow P} \propto n_{i-2\uparrow P}\left(1-n_{i-1\uparrow P}\right) = \\ &J_{i-1,i\uparrow P} \propto n_{i\uparrow P}\alpha \end{aligned} \tag{9}$$

where the TSP of both electrodes is taken to be equal to p, and we define $\alpha = \frac{1}{2}(1+p)$, and $\beta = \frac{1}{2}(1-p)$. To avoid unnecessary complication, we have set the exponential tunnel transmission probability connecting each of the states $n\ldots$ equal to 1, since it drops out of the expression for the JMR anyway. Equivalent sets of equations can be formulated for spin down electrons (substituting $\alpha \rightarrow \beta$ for both electrodes), as well as the antiparallel magnetization configuration (substituting $\alpha \leftrightarrow \beta$ for only one electrode).

It is easy to see that a solution that fulfils $0 < n < 1$ for the antiparallel configuration is $n\ldots_{\uparrow AP} = \beta$ and $n\ldots_{\downarrow AP} = \alpha$, for an arbitrary number of sequential tunneling events (here we use the convention that the sign of the TSP of electrode (0) is changed when changing from a parallel to an antiparallel configuration). In fact, it turns out that this is the only solution for the AP configuration. Regardless of the amount of tunnel steps, the AP currents thus become $J_{\uparrow AP} = J_{\downarrow AP} \propto \alpha\beta$. The solutions for $n\ldots_P$ are more complicated, but can nevertheless be evaluated analytically for $i \leq 3$, while we use a simple graphical procedure for $i = 4$ to solve the equation for $n\ldots_P$ including terms $(n\ldots_P)^3$. The so obtained curves for J_P and J_{AP} as a function of the tunnel spin polarization p of the electrodes are shown in **Figure 3**a, while the JMR as a function of the number of tunneling steps for $p = 0.3$ is shown in Figure 3b.

These calculations show that the magnetoresistance continues to drop upon the inclusion of additional tunneling steps, as may be intuitively expected. This leads to an overall junction resistance that becomes more and more spin-independent, which is qualitatively similar to the conductivity mismatch problem in the diffusive regime.[5] In a more realistic approach, one should consider also events with unequal transmission coefficients for inbound and outbound tunneling, as well as back-tunneling events, which will further strongly reduce the JMR. It is important to note at this point that we have not yet included any effects of a finite spin lifetime in the intermediate states (which certainly plays a role in reality); the reduction of the magnetoresistance discussed above is solely due to the requirement of continuity of the tunnel current, which determines the spin-dependent occupation numbers, and therefore the JMR.

2.3.2. Interfacial Tunneling Sites Connected via a Large Number of Uncorrelated Hops

We consider the case of two sites n_1 and n_2 at a distance d from each opposing FM electrode (both electrodes having a TSP equal to p) connected via different pathways involving a large number of (uncorrelated) hops via localized sites in the C_{60} layer. If we allow (thermally activated) hopping via a large number of different sites, electrons will travel via an ensemble of random paths and keeping track of the spin

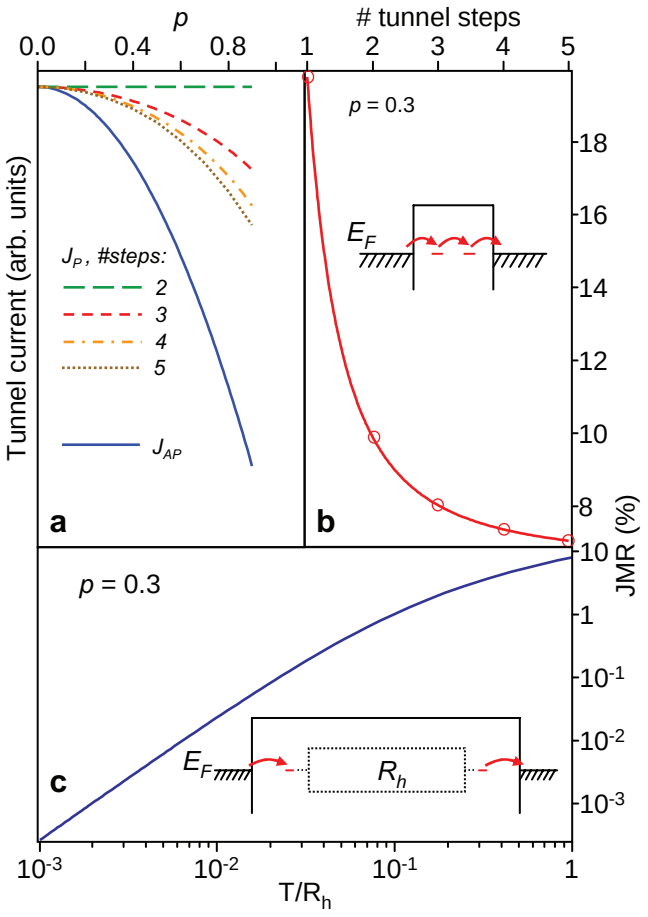

Figure 3. a) Calculated relative tunnel currents in the parallel (J_P) and antiparallel (J_{AP}) magnetization configuration for different numbers of tunneling steps as a function of the tunnel spin polarization p in both ferromagnetic electrodes. b) JMR as a function of the number of tunnel steps for $p = 0.3$. The solid line is a guide to the eye and the inset depicts a three-step tunneling process. c) JMR versus the ratio of the transmission probability T for tunneling into/out-of interfacial states and the dimensionless constant R_h proportional to the bulk hopping resistivity.

dependent occupation numbers of neighboring sites is no longer very meaningful. Instead, we may model the transmission between the sites as $1/R_h$, with R_h a dimensionless constant that is proportional to the (spin independent) electrical resistivity of the C_{60} layer in the hopping transport regime. The set of equations to be solved for obtaining the n's and J's then becomes:

$$\begin{aligned} J_{01\uparrow P} &\propto \alpha\left(1-n_{1\uparrow P}\right)T \\ &= J_{12\uparrow P} \propto n_{1\uparrow P}\left(1-n_{2\uparrow P}\right)1/R_h \\ &= J_{23\uparrow P} \propto n_{2\uparrow P}\alpha T \end{aligned} \tag{10}$$

where $T = e^{-\gamma d}$ denotes the transmission probability for tunneling into/out-of states n_1 and n_2. Again, similar equations should be solved for the different spin currents and magnetization configurations. Since only tunneling to/from the sites close to the barrier is spin dependent, the JMR continues to drop upon increasing R_h (see Figure 3c).

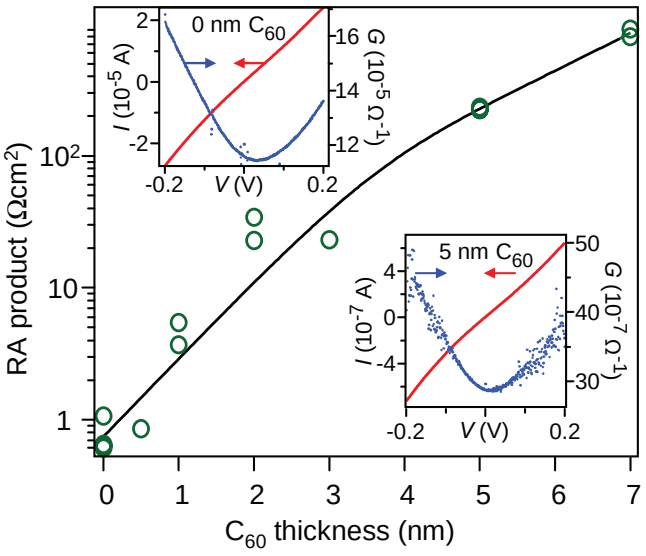

Figure 4. RA product (open circles) of a set of junctions with increasing C_{60} thickness measured at room temperature and 20 mV bias voltage. The insets show room temperature I–V and conductance (G) curves of a reference device without C_{60} interlayer (upper left corner) and a junction with a 5 nm thick C_{60} layer (lower right corner).

3. Magnetotransport Experiments

3.1. Resistance and JMR versus C_{60} Thickness

Upon increasing the C_{60} thickness stepwise from 0 to 7 nm, the resistance of our junctions increases strongly, as expected for devices in which transport is limited by tunneling. Above a thickness of 2–3 nm, the resistance increase with d_C levels off, as two-step tunneling via an intermediate state in the C_{60} layer becomes the dominant transport mechanism instead of direct tunneling between the Co and NiFe electrodes (see **Figure 4**). The solid line is obtained by a fit in which the current is composed of a weighted average of direct tunneling and two-step tunneling contributions (Equation 1 of ref. [19]). For the Al_2O_3 barrier, we estimate an extinction coefficient of evanescent states $\kappa \approx 3$ nm^{-1}, based on measurements of the resistance area product as a function of thickness of similar Al_2O_3 tunnel contacts,[31] while the thickness of the barrier d_A is 2 nm. These parameters are inserted into the fit function, which yields $\gamma \approx 1.36$ nm^{-1} for the extinction coefficient in C_{60}, and $N = 4.6 \times 10^{-4}$ nm^{-1} for the weighting factor that determines the relative contributions of direct and two-step tunneling events. The latter is proportional to the density of intermediate states within the C_{60} layer (hence the dimension nm^{-1}), via which two-step tunneling may proceed. These parameters are used below in calculations of, e.g., the JMR. The current–voltage (I–V) and conductance $G = \mathrm{d}I/\mathrm{d}V$ characteristics (see insets in Figure 4 for room-temperature measurements), as well as their temperature dependence (Supporting Information Figure S1), are consistent with tunneling being the limiting mechanism for charge transport.

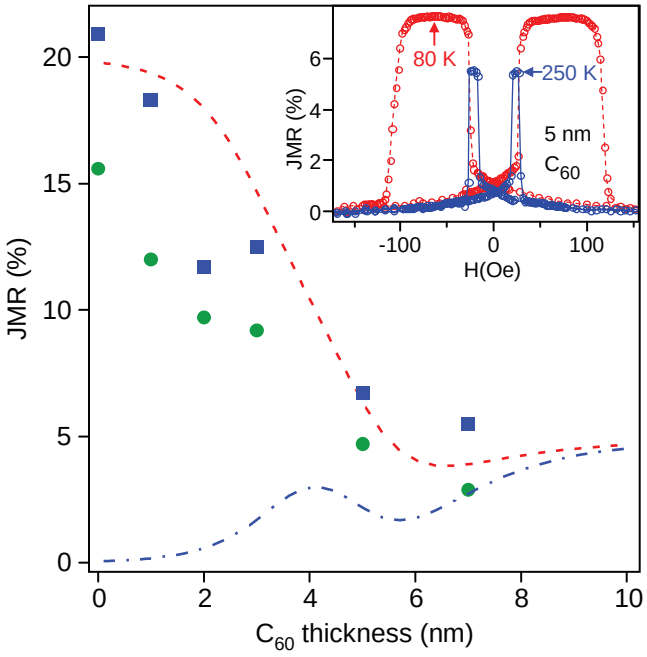

Figure 5. JMR as a function of C_{60} thickness. Data points are shown for measurements performed at room temperature (solid circles) and 5 K (solid squares). The dashed line is the calculated JMR for a combination of direct- and two-step tunneling, while the dash-dotted line corresponds to two-step tunneling only. The inset shows traces of the resistance versus magnetic field of a junction with 5 nm C_{60} (plotted as a JMR value), measured at 250 K (blue) and 80 K (red).

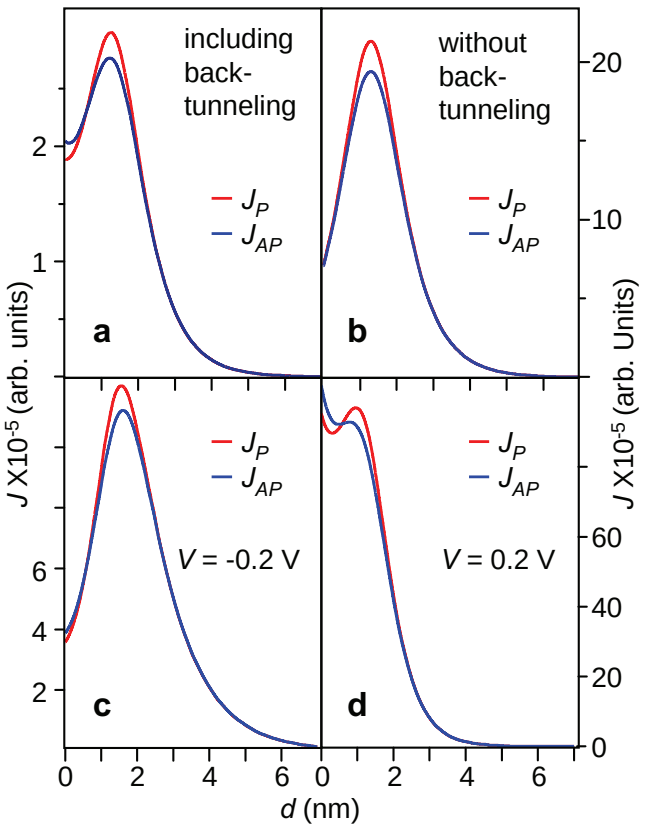

Figure 6. Calculated relative two-step tunneling current densities as a function of the distance d of the involved intermediate states from the Al_2O_3 barrier, for a 7 nm thick C_{60} layer. a) Two-step tunneling current density including back tunneling. b) Same as (a), but without back tunneling. c) Two-step tunneling current density calculated with a Gaussian energy distribution of intermediate states and a negative bias voltage of 200 mV. d) Same as (c), but with a positive bias voltage of 200 mV.

The magnetoresistance of the junctions, measured at room temperature (293 K) and 5 K at a bias voltage of 20 mV, is plotted versus the C_{60} thickness in **Figure 5**. The inset shows traces of the resistance versus the magnetic field of a device with 5 nm C_{60} measured at 250 K and 80 K. Also shown are calculated JMR curves for a superposition of direct and two-step tunneling (dashed line), and two-step tunneling only (dash-dotted line). In the calculations, we have set the tunnel spin polarization (TSP) for both ferromagnetic electrodes equal to 0.3, which is close to the experimentally obtained values for Co/Al_2O_3 and NiFe/Al_2O_3.[31–33] It is evident that the inclusion of a C_{60} layer in the MTJ stack leads to a reduction of the JMR, due to tunneling via intermediate states in the C_{60} for $d_C \geq 2$, and a somewhat reduced TSP at the NiFe/C_{60} interface compared to that of NiFe/Al_2O_3, leading to a modest reduction of the JMR even for C_{60} layers as thin as 1 nm. Junctions with 0.5 nm C_{60}, well below the threshold for closed-layer formation, show a JMR identical to that of reference MTJs without C_{60}, which is to be expected since the tunnel current will flow predominantly in those regions of the junction where the C_{60} is absent. For C_{60} layers with a thickness above 1 nm, the reduced JMR thus indicates that tunneling of electrons across a composite Al_2O_3/C_{60} is the dominant transport mechanism. The calculated JMR curves in Figure 5 predict a reduction of the magnetoresistance by about a factor of 4 in the two-step tunneling regime (d_C = 5 and 7 nm) as compared to direct tunneling across an Al_2O_3/C_{60} barrier ($d_C \leq 1$ nm), which is fairly consistent with the experimental data. The calculated JMR due to two-step tunneling alone (the dash-dotted line in Figure 5) shows some additional features. The very low JMR for small C_{60} thickness is due to the fact that the tunnel current via the intermediate site is determined by the transmission through the Al_2O_3 barrier, such that the site occupation numbers are always fairly similar regardless of the electron spin or the magnetization configuration (parallel or antiparallel).[19] The dip in the two-step JMR curve at intermediate thickness is due to back-tunneling processes, which lead to a significantly higher forward tunneling rate in the antiparallel state than the parallel state for sites close to the Al_2O_3 electrode for intermediate C_{60} thickness (see **Figure 6**a,b).

We have also studied junctions comprising considerably thicker C_{60} interlayers, with d_C = 10 and 20 nm. These devices exhibit strongly non-linear *I–V* curves (Supporting Information Figure S2), similar to those observed previously for C_{60}-based spin valves with relatively high C_{60} thickness,[12,13] which is indicative for transport limited by bulk hopping conduction instead of tunneling via a small number of intermediate steps. We do not observe any (room-temperature) magnetoresistance in these devices, consistent with calculations of the JMR as a function

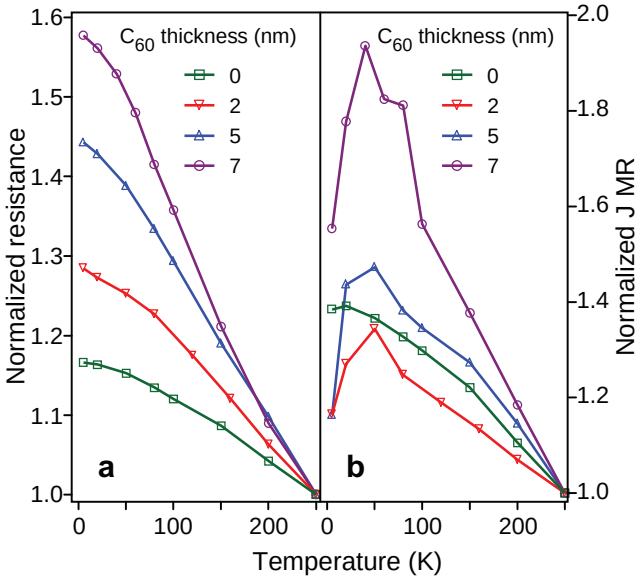

Figure 7. Temperature dependence of the resistance and JMR. a) Normalized resistance versus temperature of junctions with different C_{60} thickness between 0 and 7 nm. b) Normalized JMR of the same junctions as in (a).

of an increasing amount of intermediate tunneling steps (see Figure 3a,b), and with the notion that the JMR becomes negligible when the hopping resistivity dominates charge transport across the junction (see Figure 3c). A very important conclusion is that the observation of a vanishing magnetoresistance at a certain thickness of an organic interlayer can not be simply used to estimate the spin diffusion length in that layer. Even for an infinitely long spin diffusion length, our analysis shows that the JMR will decay to negligible values if the number of tunneling steps becomes sufficiently large.

3.2. Temperature Dependence of the Resistance and JMR

The normalized device resistance as a function of temperature is shown in **Figure 7**a. The stronger temperature dependence of the resistance and JMR for junctions with larger d_C shows that thermal activation becomes more important in those junctions, consistent with tunneling via one or more intermediate states. Interestingly, the JMR of junctions with $d_C \geq 2$ nm shows a non-monotonic dependence on temperature (see Figure 7b); in particular for the junctions with d_C equal to 5 and 7 nm, the JMR shows a clear maximum at 50 K. This suggests that the temperature dependence of the JMR is affected by competing mechanisms. The first mechanism, responsible for the decreasing JMR with T for $T > 50$ K, is ascribed to the larger contribution of thermally activated two- (or multi-) step tunneling processes with increasing temperature. For the second mechanism, spin relaxation and dephasing during occupation of the intermediate site in the C_{60} layer is the most probable candidate. The outbound tunneling frequency from the intermediate state can be estimated as $\nu_0 \exp\left(-2d\sqrt{2m_e U}/\hbar\right)$, where ν_0 is the (material dependent) phonon attempt frequency, U is the barrier height, d is the barrier width, and m_e the effective mass. The effective barrier height is reduced when the electrons gain thermal energy in the intermediate state. This leads to a higher tunneling frequency, analogous to hopping transport in organic semiconductors.[25,34] The dwell time of the electrons in the intermediate states will thus increase as the temperature is reduced, which affects the spin relaxation and dephasing in the intermediate site(s). As discussed above, hyperfine interactions are very small in C_{60}[22,23] and are thus unlikely to play an important role. The importance of spin orbit (SO) coupling for spin relaxation in organic semiconductors is currently under hot debate. Up until recently, the consensus was that SO interactions, which scale with the fourth power of the atomic number, are too weak to be of major importance in organic materials. However, recent theoretical studies have cast doubts on this view.[35,36] In the work of Yu,[36] the SO coupling was found to be strongly dependent on the molecular structure. To our knowledge, no computational studies of the SO coupling strength in C_{60} are available at this time, such that a quantitative estimate of the associated spin relaxation effects cannot be given.

Here, we propose a third mechanism that may limit the spin polarization in the intermediate states, namely spin precession in local, inhomogeneous magnetostatic fields arising from the finite roughness at the interfaces with the ferromagnetic electrodes.[37,38] Such fields are well known to affect the switching behavior of metal/insulator/metal magnetic tunnel junctions, in what is usually referred to as Néel or "orange peel" coupling.[39,40] In addition, it has been shown recently that roughness-induced fields play a significant role in spin relaxation at interfaces between ferromagnet/tunnel-barrier contacts and silicon.[38] Since the fields are inhomogeneous in magnitude as well as in direction, the resulting random precession of electron spins will lead to a decay of the spin polarization in the intermediate state, if the (temperature-dependent) two-step tunneling frequency becomes comparable to the Larmor spin precession frequency. The latter is equal to $g\mu_B B/h$ s^{-1} where g is the spin gyromagnetic ratio, μ_B is the Bohr magneton, B is the inhomogeneous magnetostatic field, and h is Planck's constant.

In our junctions, the intermediate sites involved in two-step (or multistep) tunneling are located at several nm from the interfaces with the ferromagnets. For a peak-to-peak roughness amplitude of 0.5 to 1 nm, similar to the interfacial roughness in our devices (see Supporting Information Figure S3), calculations by Dash et al.[38] show that the local magnetostatic fields are of the order of 100 mT at a distance of up to 10 nm away from the interface. It should be pointed out in passing that in our case not one but two ferromagnetic interfaces are present, such that the local magnetic fields and the associated precession frequency might be even higher than for the Si-based devices studies by Dash et al. The corresponding Larmor precession frequency is of the order of 10^9 Hz. It is interesting to compare this precession frequency, which sets the timescale for spin relaxation in local roughness-induced fields, to an estimate of the tunneling frequency. The two-step tunneling processes in our devices involve a distribution of intermediate sites with different tunneling distances d, resulting in a distribution of different tunneling rates (see Figure 6). For junctions with

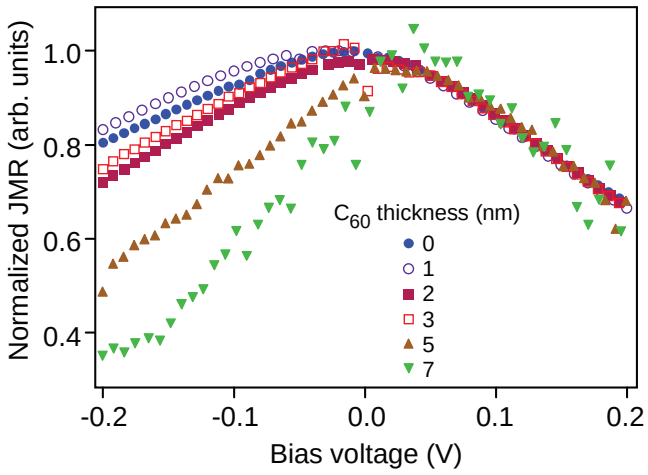

Figure 8. Bias dependence of the JMR. Normalized JMR measurements are shown, measured at $T = 200$ K, as a function of bias voltage for junctions with different C_{60} interlayer thickness.

7 nm C_{60}, the peak of the tunneling rate distribution occurs for intermediate sites located about 1 nm from the Al_2O_3/C_{60} interface. The corresponding tunneling rate ν_{tun} can be estimated as $\nu_{tun} = \nu_0 \exp(-^{\gamma d})$, where $d \approx 6$ nm is the outbound tunneling distance, $\gamma = 1.36$ nm^{-1} is the extinction coefficient in C_{60} obtained from the fit in Figure 4, and ν_0 is the phonon attempt frequency. The latter can be estimated as 10^{13} Hz, based on studies of the frequencies of vibrational modes that couple to the LUMO orbitals of C_{60}.[41,42] Hence, we find a tunneling frequency of the order of 10^9 Hz, similar to the precession frequency associated with the local roughness-induced fields. For junctions with 5 nm C_{60}, two-step tunneling occurs mostly for intermediate states close to the Al_2O_3/C_{60} interface, such that the relevant outbound tunneling distance is about 5 nm, and $\nu_{tun} \approx 10^{10}$ Hz. Since the timescales for two-step tunneling and relaxation are similar, and the effective barrier height depends on temperature as discussed above, the scenario sketched above is entirely consistent with our observation of a maximum in the temperature dependence of the JMR.

3.3. Bias Voltage Dependent Properties

We now address the evolution of the JMR versus bias voltage for junctions with different C_{60} thickness between 0 and 7 nm (see **Figure 8**), obtained from I–V curves measured in the parallel and antiparallel magnetization configurations. For the junctions with 5 and 7 nm C_{60}, applying larger negative bias voltages (electrons tunneling from Co to NiFe) results in a considerably faster reduction of the JMR as compared to junctions with thinner C_{60} layers. This suggests that two-step tunneling via intermediate sites in the C_{60} layer, which contributes more strongly for thicker layers, affects the JMR significantly for negative bias voltages, but not for positive bias voltages. Note that since the JMR-versus-bias curves are all similar for junctions with thin (≤3 nm) C_{60} layers, these effects cannot be due solely to changes in the spin-polarized interfacial density of states introduced by replacing the Al_2O_3/NiFe interface with C_{60}/NiFe, which would also influence the JMR of direct tunneling events.

As shown in Figure 6c,d, changing the bias voltage from –0.2 V to 0.2 V introduces a significant asymmetry in the spatial distribution of the intermediate states via which the two-step tunneling transport takes place, due to the Gaussian energy distribution of states in the gap of C_{60} (see also Figure 2a,b). At negative (positive) bias voltages, the distribution of intermediate states that participate considerably to two-step tunneling shifts away from (towards) the Al_2O_3 interface. This influences the precession of spins in the inhomogeneous magnetostatic fields resulting from the finite roughness at the ferromagnetic interfaces. Since the C_{60}/NiFe interface has a considerably larger roughness amplitude (see Supporting Information Figure S3) than the Co/Al_2O_3 interface, the redistribution of the active two-step tunneling sites towards the C_{60}/NiFe interface at sufficiently high negative bias might result in higher spin precession frequencies, and thus a larger reduction of the spin polarization in the intermediate state. To test this hypothesis, we have measured magnetoresistance hysteresis loops at $T =$ 5 K and at different bias voltages between –0.2 and 0.2 V for a junction with 5 nm C_{60} (**Figure 9**a,b). Upon application of an external magnetic field aligned with the magnetization direction of the ferromagnets, and thus with the spin polarization of the tunneling electrons, the initially random spin precession axis will rotate in the direction of the spin polarization vector since the spins precess around the vector sum of the applied field and the local magnetostatic field. Hence, spin precession in inhomogeneous local fields should be suppressed at

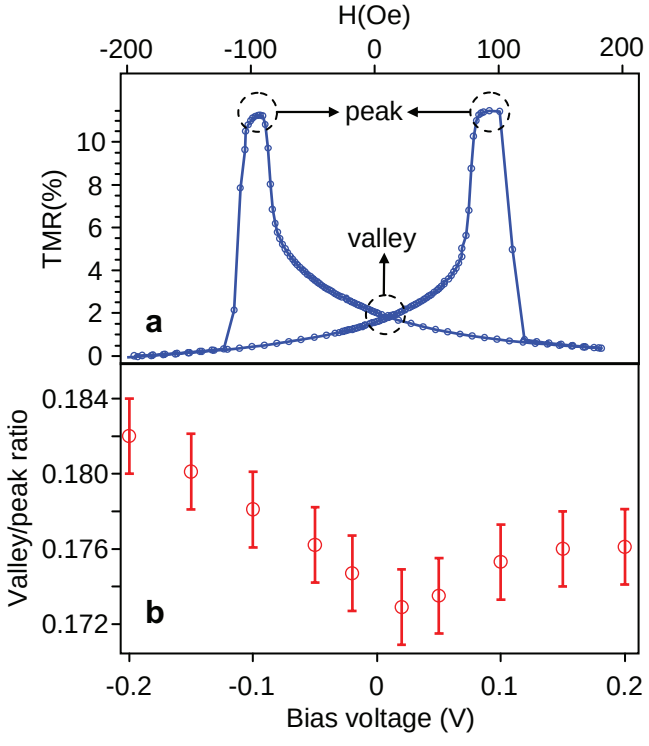

Figure 9. Bias voltage dependence of the MR traces. a) MR curve of a junction with 5 nm C_{60} measured at $T = 5$ K and a bias voltage of 20 mV, where the valley and peak values are indicated by arrows. b) Valley-to-peak ratio versus bias voltage. The error bars give a conservative estimate of the uncertainty of determining the valley and peak values.

sufficiently large external field strengths. This affects the JMR curves of the junctions in a similar way as described earlier for spin precession in local hyperfine fields (Figure 4 of ref. [19]). Small changes in the shape of the JMR curves of the junction with 5 nm C_{60} were observed upon varying the bias voltage stepwise from –0.2 to 0.2 V, which indeed points to stronger local inhomogeneous magnetostatic fields resulting in more pronounced spin precession effects.

4. Conclusions

We have presented a joint experimental and modeling study of C_{60}-based spin valves and interpreted their behavior using a superposition of direct and multistep tunneling via a Gaussian DOS of intermediate states. We find that, analogous to conductivity mismatch in the diffusive regime, the JMR drops continuously as the amount of intermediate tunneling steps increases, irrespective of the spin lifetime and spin diffusion length. Consequently, these parameters cannot be extracted simply from the thickness dependence of the JMR of organic spin valves, as has been common practice in the past (see ref. [6,7] and the references therein). Previously reported values of the spin diffusion length in organic semiconductors thus may have been strongly underestimated.

In addition to the intrinsic loss of the JMR due to multistep tunneling, our temperature- and bias-dependent measurements of the magnetotransport properties indicate that spin relaxation and dephasing in the intermediate states on the C_{60} molecules also affect the JMR. We propose that the mechanism that underlies this is spin precession in the inhomogeneous magnetostatic fields that arise from finite roughness at the ferromagnetic interfaces, which is supported by measurements of JMR versus magnetic field, recorded at different bias voltages.

Our findings are widely applicable to organic spin valves operating in the multistep tunneling regime, with a not too large amount of intermediate hops. Indeed, even for devices with relative large organic layer thickness (on the order of 100 nm), this description may be a good starting point for modeling the device behavior. Such devices unexceptionally show a very strong temperature dependence of the magnetoresistance,[7] which is most probably related with the reduction of the hopping rate, and hence the number of hops involved in transport, at low temperature. We expect that further theoretical analysis, for example using Monte Carlo/master equation approaches, will provide additional insights into the operation of these fascinating and promising devices.

5. Experimental Section

Device Fabrication: Our devices were prepared in situ in an ultrahigh vacuum chamber (base pressure 10^{-10} mbar). Metals were deposited by electron-beam evaporation (rate ≈ 1 Å s^{-1}), and C_{60} was evaporated from a Knudsen cell at ≈400 °C (rate ≈ 0.25 Å s^{-1}). The layer stacks were grown onto single-crystalline Al_2O_3 substrates (11 × 11 mm^2) held at room temperature. Twelve identical junctions, with an area of 0.25 × 0.3 mm^2, were fabricated on each substrate in a cross-bar geometry using shadow masks. The junctions consisted of the following layer stack: Co(bottom, 8 nm)/Al_2O_3(2 nm)/C_{60}(d_C nm)/$Ni_{81}Fe_{19}$(15 nm). Reference magnetic tunnel junctions, without C_{60}, were fabricated in parallel with C_{60}-containing junctions in every run (the apparatus allowed for parallel fabrication of several devices with different layer structure using shadow masks). The Al_2O_3 tunnel barriers were formed by depositing 1.5 nm Al, followed oxidation in an oxygen plasma at 100 mTorr, without breaking vacuum. Film thickness was monitored by quartz crystal oscillators and verified with atomic force microscopy (AFM) measurements.

Measurements: The surface morphology was characterized by AFM. Junction resistances versus magnetic field (*R*–*H*) at different bias voltages, and current–voltage (*I*–*V*) measurements at constant applied magnetic field (corresponding to parallel- and antiparallel magnetization of top and bottom electrodes) were measured using a four-point probe technique. The measurements were performed within a temperature range from room temperature to 5 K using a liquid He flow cryostat.

Supporting Information

Supporting Information is available from the Wiley Online Library or from the author.

Acknowledgements

The authors acknowledge financial support from the NWO VIDI program, grants no. 10246 and 07580, and the European project MINOTOR, grant no. FP7-NMP-228424.

Received: October 26, 2011
Published online: January 31, 2012

[1] I. Zutic, J. Fabian, S. Das Sarma, *Rev. Mod. Phys.* **2004**, *76*, 323.
[2] J. Fabian, A. Matos-Abiague, C. Ertler, P. Stano, I. Zutic, *Acta Phys. Slovaca* **2007**, *57*, 565.
[3] S. P. Dash, S. Sharma, R. S. Patel, M. P. de Jong, R. Jansen, *Nature* **2009**, *462*, 491.
[4] A. Fert, H. Jaffres, *Phys. Rev. B* **2001**, *64*, 184420.
[5] G. Schmidt, D. Ferrand, L. W. Molenkamp, A. T. Filip, B. J. van Wees, *Phys. Rev. B* **2000**, *62*, R4790.
[6] W. J. M. Naber, S. Faez, W. G. van der Wiel, *J. Phys. D: Appl. Phys.* **2007**, *40*, R205.
[7] V. Dediu, L. E. Hueso, I. Bergenti, C. Taliani, *Nat. Mater.* **2009**, *8*, 707.
[8] V. Dediu, M. Murgia, F. C. Matacotta, C. Taliani, S. Barbanera, *Solid State Commun.* **2002**, *122*, 181.
[9] C. B. Harris, R. L. Schlupp, H. Schuch, *Phys. Rev. Lett.* **1973**, *30*, 1019.
[10] V. I. Krinichnyi, S. D. Chemerisov, Y. S. Lebedev, *Phys. Rev. B* **1997**, *55*, 16233.
[11] Z. H. Xiong, D. Wu, Z. V. Vardeny, J. Shi, *Nature* **2004**, *427*, 821.
[12] M. Gobbi, F. Golmar, R. Llopis, F. Casanova, L. E. Hueso, *Adv. Mater.* **2011**, *23*, 1609.
[13] R. Lin, F. J. Wang, M. Wohlgenannt, C. Y. He, X. F. Zhai, Y. Suzuki, *Synth. Met.* **2011**, *161*, 553.
[14] T. D. Nguyen, G. Hukic-Markosian, F. J. Wang, L. Wojcik, X. G. Li, E. Ehrenfreund, Z. V. Vardeny, *Synth. Met.* **2011**, *161*, 598.
[15] V. Dediu, L. E. Hueso, I. Bergenti, A. Riminucci, F. Borgatti, P. Graziosi, C. Newby, F. Casoli, M. P. de Jong, C. Taliani, Y. Zhan, *Phys. Rev. B* **2008**, *78*, 115203.
[16] C. Barraud, P. Seneor, R. Mattana, S. Fusil, K. Bouzehouane, C. Deranlot, P. Graziosi, L. Hueso, I. Bergenti, V. Dediu, F. Petroff, A. Fert, *Nat. Phys.* **2010**, *6*, 615.

[17] A. J. Drew, J. Hoppler, L. Schulz, F. L. Pratt, P. Desai, P. Shakya, T. Kreouzis, W. P. Gillin, A. Suter, N. A. Morley, V. K. Malik, A. Dubroka, K. W. Kim, H. Bouyanfif, F. Bourqui, C. Bernhard, R. Scheuermann, G. J. Nieuwenhuys, T. Prokscha, E. Morenzoni, *Nat. Mater.* **2009**, *8*, 109.
[18] R. Lin, F. Wang, J. Rybicki, M. Wohlgenannt, K. A. Hutchinson, *Phys. Rev. B* **2010**, *81*, 195214.
[19] J. J. H. M. Schoonus, P. G. E. Lumens, W. Wagemans, J. T. Kohlhepp, P. A. Bobbert, H. J. M. Swagten, B. Koopmans, *Phys. Rev. Lett.* **2009**, *103*, 146601.
[20] J. S. Jiang, J. E. Pearson, S. D. Bader, *Phys. Rev. B* **2008**, *77*, 035303.
[21] P. A. Bobbert, T. D. Nguyen, F. W. A. van Oost, B. Koopmans, M. Wohlgenannt, *Phys. Rev. Lett.* **2007**, *99*, 216801.
[22] D. Zhang, J. R. Norris, P. J. Krusic, E. Wasserman, C. C. Chen, C. M. Lieber, *J. Phys. Chem.* **1993**, *97*, 5886.
[23] T. D. Nguyen, Y. Sheng, M. Wohlgenannt, T. D. Anthopoulos, *Synth. Met.* **2007**, *157*, 930.
[24] B. Hartenstein, H. Bassler, *J. Non-Cryst. Solids* **1995**, *190*, 112.
[25] R. Coehoorn, W. F. Pasveer, P. A. Bobbert, M. A. J. Michels, *Phys. Rev. B* **2005**, *72*, 155206.
[26] P. Rudolf, M. S. Golden, P. A. Brühwiler, *J. Electron. Spectrosc. Relat. Phenom.* **1999**, *100*, 409.
[27] S. Braun, W. R. Salaneck, M. Fahlman, *Adv. Mater.* **2009**, *21*, 1450.
[28] R. W. Lof, M. A. van Veenendaal, B. Koopmans, H. T. Jonkman, G. A. Sawatzky, *Phys. Rev. Lett.* **1992**, *68*, 3924.
[29] W. Osikowicz, M. P. de Jong, W. R. Salaneck, *Adv. Mater.* **2007**, *19*, 4213.
[30] M. Popinciuc, H. T. Jonkman, B. J. van Wees, *J. Appl. Phys.* **2007**, *101*, 093701.
[31] B. C. Min, PhD Thesis, University of Twente, Enschede, **2007**.
[32] T. S. Santos, J. S. Lee, P. Migdal, I. C. Lekshmi, B. Satpati, J. S. Moodera, *Phys. Rev. Lett.* **2007**, *98*, 016601.
[33] B. C. Min, K. Motohashi, J. C. Lodder, R. Jansen, *Nat. Mater.* **2006**, *5*, 817.
[34] A. Miller, E. Abrahams, *Phys. Rev.* **1960**, *120*, 745.
[35] S. Bandyopadhyay, *Phys. Rev. B* **2010**, *81*, 153202.
[36] Z. G. Yu, *Phys. Rev. Lett.* **2011**, *106*, 106602.
[37] S. Demokritov, E. Tsymbal, P. Grünberg, W. Zinn, I. K. Schuller, *Phys. Rev. B* **1994**, *49*, 720.
[38] S. P. Dash, S. Sharma, J. C. Le Breton, J. Peiro, H. Jaffrès, J. M. George, A. Lemaître, R. Jansen, *Phys. Rev. B* **2011**, *84*, 054410.
[39] J. C. S. Kools, W. Kula, D. Mauri, T. E. Lin, *J. Appl. Phys.* **1999**, *85*, 4466.
[40] B. D. Schrag, A. Anguelouch, S. Ingvarsson, G. Xiao, Y. Lu, P. L. Trouilloud, A. Gupta, R. A. Wanner, W. J. Gallagher, P. M. Rice, S. S. P. Parkin, *Appl. Phys. Lett.* **2000**, *77*, 2373.
[41] D. S. Bethune, G. Meijer, W. C. Tang, H. J. Rosen, W. G. Golden, H. Seki, C. A. Brown, M. S. Devries, *Chem. Phys. Lett.* **1991**, *179*, 181.
[42] J. L. Janssen, M. Cote, S. G. Louie, M. L. Cohen, *Phys. Rev. B* **2010**, *81*, 073106.